

# Discovery of Kolmogorov-like Magnetic Energy Spectrum in Tycho’s Supernova Remnant by Two-point Correlations of Synchrotron Intensity

Jiro Shimoda,<sup>1,2\*</sup> Takuya Akahori<sup>3</sup> A. Lazarian,<sup>4</sup> Tsuyoshi Inoue,<sup>5</sup> and Yutaka Fujita<sup>6</sup>

<sup>1</sup>*Department of Physics and Mathematics, Aoyama-Gakuin University, Sagamihara, Kanagawa 252-5258, Japan*

<sup>2</sup>*Frontier Research Institute for Interdisciplinary Sciences, Tohoku University, Sendai 980-8578, Japan*

<sup>3</sup>*Mizusawa VLBI Observatory, National Astronomical Observatory of Japan, 2-12 Hoshigaoka, Mizusawa, Oshu, Iwate 023-0861, Japan*

<sup>4</sup>*Department of Astronomy, University of Wisconsin, 475 North Charter Street, Madison, WI 53706, USA*

<sup>5</sup>*Department of Physics, Graduate School of Science, Nagoya University, Furo-cho, Chikkusa-ku, Nagoya 464-8602, Japan*

<sup>6</sup>*Department of Earth and Space Science, Graduate School of Science, Osaka University, Toyonaka, Osaka 560-0043, Japan*

Accepted XXX. Received YYY; in original form ZZZ

## ABSTRACT

The spectral slope of the magnetic energy in supernova remnants (SNRs) can be obtained by analysis of spatial two-point correlation functions of synchrotron intensities. This method has been originally developed for the analysis of magnetic field structure in diffuse interstellar medium and applied when the geometry of the emission region is simple and known. In this paper, applying this correlation analysis to Tycho’s SNR, for which the synchrotron emission region is known to be a spherical shell, we find that the magnetic energy spectrum shows the Kolmogorov-like scaling. Our results can be explained by turbulence developed downstream of the shock front via Richtmyer-Meshkov instability or an amplification of upstream magnetic field induced by cosmic rays. They could be discriminated by future observations with a sub arcsecond resolution such as Square Kilometer Array.

**Key words:** ISM: supernova remnants—acceleration of particles—turbulence—magnetic fields—(*magnetohydrodynamics*) MHD—shock waves

## 1 INTRODUCTION

Supernova remnant (SNR) shock waves are believed to be an accelerator of Galactic cosmic-rays (CRs) with energies at least up to  $10^{15.5}$  eV (called “knee energy”). However, there is no firm evidence that the SNRs are accelerators of the knee-energy CRs. In the standard scenario, the CR particles are accelerated through the “diffusive shock acceleration” (DSA) mechanism (e.g. Blandford & Ostriker 1978; Bell 1978) which is accompanied by simultaneous generation of magnetic-field disturbances at the vicinity of the shocks (e.g. Bell 2004). In the DSA mechanism, CR particles are scattered through interactions with the field disturbances to go back and forth between upstream and downstream of the shock, suffering the shock heating repeatedly and increasing their energy. If the mean free path of the accelerated particles is sufficiently larger than a radius of the SNR, they escape from the SNR shock and the acceleration is finished. Thus, the maximum energy of the accelerated

particles depends on their diffusion coefficient. If we consider a monochromatic field disturbance with scale length  $l$ , a CR particle with gyroradius  $r_g \simeq l$  interacts resonantly with the monochromatic field disturbance resulting in a pitch-angle scattering (Jokipii 1966). The strength of the scattering depends on an energy density of the magnetic field disturbance. Because the field disturbance usually has a continuous energy spectrum due to a turbulent cascade, the CR particles with different energies resonate with the field disturbances at different scale lengths. Hence, the diffusion coefficient and the maximum energy are related to the spectrum. For the field disturbances with an energy spectrum proportional to  $l^m$ , the diffusion coefficient of the particles with energy  $E$  can be written as

$$\kappa(E) \sim \bar{\kappa}(E_0) \left( \frac{E}{E_0} \right)^{1-m}, \quad (1)$$

where  $E_0$  is the energy of the CR particle giving the representative diffusion coefficient  $\bar{\kappa}(E_0) = cr_g(E_0)/3$  (see, e.g. Blandford & Eichler 1987; Parizot et al. 2006).  $c$  is the speed of light. Parizot et al. (2006) evaluated the maximum energy of CR protons as a function of the spectral slope  $m$  for a number of SNRs (Cas A, Kepler, Tycho, SN 1006 and

\* E-mail: s-jiro@phys.aoyama.ac.jp, j-shimoda@astr.tohoku.ac.jp (JS)

G347.3-0.5) by deriving the magnetic-field strength from the thickness of non-thermal X-ray filaments. For Tycho's SNR, if  $m \sim 2/3$  (corresponding to Kolmogorov-like turbulence), the maximum energy of CR protons reaches around the knee energy.<sup>1</sup> While the slope of the magnetic energy spectrum should be related to the maximum energy of CRs, it has not been well determined observationally. Moreover, there is a controversy over the shape of the magnetic energy spectrum realized in the SNRs such as a single power-law (e.g. Goldreich & Sridhar 1995; Cho & Vishniac 2000b), a broken power-law (e.g. Lazarian & Vishniac 1999; Cho & Vishniac 2000a; Cho & Lazarian 2003; Brandenburg & Subramanian 2005; Lazarian 2006; Beresnyak et al. 2009; Inoue et al. 2012; Xu & Lazarian 2016, 2017) and a spectrum containing several discrete peaks (Vladimirov et al. 2009). The uncertainty of the spectrum prevents us from determining the maximum energy based on the standard scenario. Therefore, it is important to obtain the spectral slope observationally to reveal acceleration process of CRs at SNRs.

It is widely recognised for interstellar medium (ISM) that the two-point correlation function of synchrotron intensities reflects statistical nature of turbulent magnetic field including the spectral slope of magnetic energy (e.g. Getmantsev 1959; Chepurnov 1998; Cho & Lazarian 2010; Lazarian & Pogosyan 2012, 2016, see also Akahori et al. (2018) for a review). This correlation analysis, however, suffers from the uncertainty of the geometry of the emission region because of the projection effect. In other words, the correlation function reflects not only the structure of the magnetic field but also the geometry of the emission region. Therefore, the geometry must be determined separately to obtain the spectral slope of magnetic energy. Fortunately, the emission region of young SNRs is often a spherical shell (e.g. Dickel et al. 1991; Reynoso et al. 2013). Thus, if we select arbitrary points on a concentric circle of an SNR image, the depth of the emission region along the line of sight through the points is constant. This means that we can exclude the geometrical effect from the correlation function. As a result, the derived correlation function depends only on the spectral slope of magnetic energy.

In this paper, we explore the spectral slope of magnetic energy in Tycho's SNR by applying the correlation analysis. This paper is constructed as follows. In section 2, we briefly explain our analysing method and the application for Tycho's SNR. The results are shown in section 3, and we discuss the origin of magnetic field structure in Tycho's SNR in section 4.

## 2 ANALYSIS OF MAGNETIC FIELD CORRELATION

To extract magnetic field correlation, we consider the second-order correlation function of the synchrotron intensity per frequency  $I_\nu$  on the circle  $S$  centred on the SNR

<sup>1</sup>  $\gamma$ -ray emissions from Tycho's SNR may originate in high energy CR protons with an energy at least  $\sim 10^{14}$  eV but there is no consensus on the maximum energy of CR protons because it depends on emission models (see Archambault et al. 2017).

centre. The function is given by

$$C_{I_\nu, S}^{(2)}(\lambda) = \frac{\int_S I_\nu(\mathbf{X}) I_\nu(\mathbf{X}') d^2\mathbf{X}}{\int_S d^2\mathbf{X}} \equiv \langle I_\nu(\mathbf{X}) I_\nu(\mathbf{X} + \lambda) \rangle_{\mathbf{X}, S}, \quad (2)$$

where  $\mathbf{X} = (x, y)$  is the two-dimensional sky position and  $\lambda = \mathbf{X}' - \mathbf{X}$  is the position vector of two separated sky positions  $\mathbf{X}$  and  $\mathbf{X}' = \mathbf{X} + \lambda$  (see Appendix A for detail). Here we select  $\mathbf{X}$  and  $\mathbf{X}' = \mathbf{X} + \lambda$  from the region

$$S(\mathbf{X}, R) = \left\{ \mathbf{X} \mid (R - \delta)^2 \leq f(x, y) \leq (R + \delta)^2 \right\}, \quad (3)$$

with  $f(x, y) = (x - x_c)^2 + (y - y_c)^2$ , where  $(x_c, y_c)$  is the centre of the SNR,  $R$  is the radius of the circle we are interested in and  $\delta \ll R$  is the width. Note that although the correlation function  $C_{I_\nu, S}^{(2)}(\lambda)$  is defined in a two-dimensional space, it is mostly represented as one-dimensional function owing to the condition  $\delta \ll R$ , that is, the domain of definition of  $C_{I_\nu, S}^{(2)}(\lambda)$  is much elongated in the azimuthal direction. For Kolmogorov-like turbulent field, the one-dimensional correlation function shows the scaling relation of  $\lambda^{2/3}$  (e.g. Kolmogorov 1941).

We study Tycho's SNR using the correlation function. We analyse a 1.4 GHz image, which is published in Williams et al. (2016), obtained by Very Large Array: project VLA/13A-426 (PI J. W. Hewitt). Figure 1 shows the image. The synthesized beam size (angular resolution) is 1.92 arcsec and the image pixel size is 0.4 arcsec. The image noise level is  $\sigma_{\text{Tycho}} = 5.3 \times 10^{-5}$  Jy beam<sup>-1</sup>. Supposing that the distance to Tycho's SNR is  $d = 4$  kpc (Hayato et al. 2010; Katsuda et al. 2010), 1 arcsec  $\approx 0.02$  pc ( $d/4$  kpc). We calculate the intensity centroid from pixels with  $I_\nu \geq 3\sigma_{\text{Tycho}}$  at the rim of SNR, and set the centre of concentric circles at the centroid: (R.A., Dec.) = ( $0^{\text{h}}25^{\text{m}}19^{\text{s}}.1, +64^{\circ}08'23''.0$ ). It mostly agrees with the geometrical centre derived from the X-ray image (Ruiz-Lapuente et al. 2004): (R.A., Dec.) = ( $0^{\text{h}}25^{\text{m}}19^{\text{s}}.9, +64^{\circ}08'18''.2$ ). We analyse eight concentric circles with radii,  $R = 1.00R_{\text{SNR}}$  (white),  $0.97R_{\text{SNR}}$  (red),  $0.94R_{\text{SNR}}$  (purple),  $0.91R_{\text{SNR}}$  (green),  $0.88R_{\text{SNR}}$  (blue),  $0.85R_{\text{SNR}}$  (light blue),  $0.82R_{\text{SNR}}$  (yellow) and  $0.79R_{\text{SNR}}$  (orange), where  $R_{\text{SNR}} = 632$  pixels  $\approx 253$  arcsec  $\approx 5$  pc is the SNR radius. The width of each circle is set to be  $\delta = 0.0091R_{\text{SNR}}$ .

Errors on the correlation function are evaluated from the lower and upper limits of  $C_{I_\nu, S}^{(2)}$ . There are pixels having weak signals of  $I_\nu < 3\sigma_{\text{Tycho}}$ . We regard such weak signals as noise. Meanwhile, if we assign a pseudo-signal of  $3\sigma_{\text{Tycho}}$  to those pixels, we obtain the maximum value of the correlation function. We regard it as the upper limit. Similarly, if we assign zero to those pixels, we obtain the minimum value as the lower limit. We regard these limits as the errors of  $C_{I_\nu, S}^{(2)}$ .

## 3 RESULTS

Figure 2 shows the second-order correlation functions  $C_{I_\nu, S}^{(2)}$ . The line width indicates the errors evaluated from the upper and lower limits of  $C_{I_\nu, S}^{(2)}$ . In order to clarify the correlation of fluctuating component, we display  $|C_{I_\nu, S}^{(2)}(\lambda) - C_{I_\nu, S}^{(2)}(\lambda_{\text{min}})|$ , where  $\lambda_{\text{min}} \approx 1.4$  arcsec is the minimum separation distance between  $\mathbf{X}$  and  $\mathbf{X}'$ .

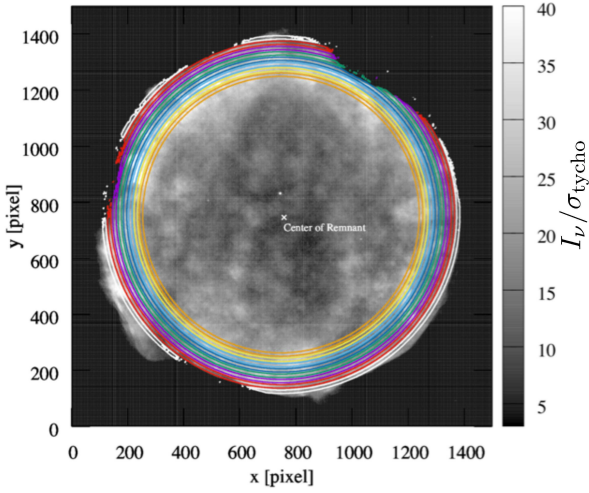


**Figure 1.** Radio synchrotron ( $I_\nu$ ) images of Tycho's SNR.  $\sigma_{\text{tycho}} = 5.3 \times 10^{-5}$  Jy beam $^{-1}$  is the image noise level.  $x$  and  $y$  axes are in units of the number of pixels (one pixel size is 0.4 arcsec). The origin of the coordinates (J2000) for Tycho's SNR is (R.A., Dec.) = ( $0^{\text{h}}25^{\text{m}}19^{\text{s}}.1, +64^{\circ}08'23''.0$ ). The regions enclosed by coloured lines (white, red, purple, green, blue, light blue, yellow and orange) indicate  $I_\nu \geq 3\sigma_{\text{tycho}}$  at each concentric circles ( $R = 1.00 R_{\text{SNR}}, 0.97 R_{\text{SNR}}, 0.94 R_{\text{SNR}}, 0.91 R_{\text{SNR}}, 0.88 R_{\text{SNR}}, 0.85 R_{\text{SNR}}, 0.82 R_{\text{SNR}}$  and  $0.79 R_{\text{SNR}}$ ).

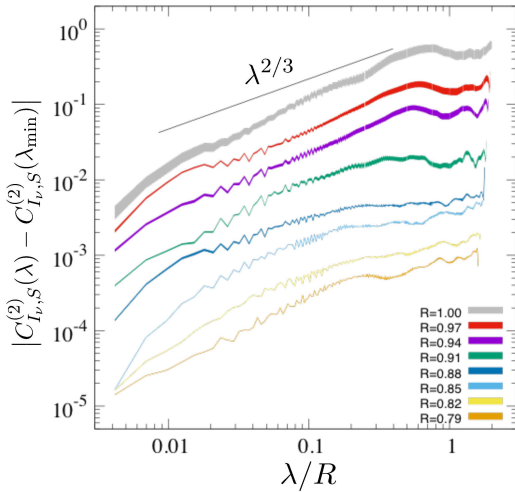


**Figure 2.** Second-order correlation functions of the observed synchrotron intensities per frequency  $I_\nu$ , which imply the spectra of magnetic energy in Tycho's SNR. To clarify the fluctuating component of the correlation, we display  $|C_{I_\nu,S}^{(2)}(\lambda) - C_{I_\nu,S}^{(2)}(\lambda_{\text{min}})|$ . The solid belts represent the normalized correlation functions evaluated along the concentric circles with radii of  $R = 1.00 R_{\text{SNR}}, 0.97 R_{\text{SNR}}, 0.94 R_{\text{SNR}}, 0.91 R_{\text{SNR}}, 0.88 R_{\text{SNR}}, 0.85 R_{\text{SNR}}, 0.82 R_{\text{SNR}}$  and  $0.79 R_{\text{SNR}}$  from top to bottom, respectively.

For the outer circles with radii  $R \geq 0.90$ ,  $C_{I_\nu,S}^{(2)}$  follows a power law and has a positive slope at relatively small scales ( $\lambda/R \lesssim 0.5$ ), i.e. larger-scale magnetic field disturbances are predominant. The slope is close to the Kolmogorov scaling  $\lambda^{2/3}$ . Such a single power-law with the Kolmogorov scaling is predicted by Goldreich & Sridhar (1995) (henceforth, GS95) as the developed magnetohydrodynamics (MHD) tur-

bulence. On the other hand, for the inner circles with radii  $R \leq 0.85$ ,  $C_{I_\nu,S}^{(2)}$  are somewhat flatter than the outer ones at relatively large scales  $\lambda/R \gtrsim 0.2$ , although a Kolmogorov-like scaling is implied in the small scales  $\lambda/R \lesssim 0.2$ . It may indicate that the nature of field disturbances varies at  $R \lesssim 0.9 R_{\text{SNR}}$ . Actually, by the combination of measurements of X-ray imaging and spectroscopy, Warren et al. (2005) found that the contact discontinuity, at which Rayleigh-Taylor instability (RTI) works, is located at  $R \approx 0.9 R_{\text{SNR}}$ .

## 4 DISCUSSION

The correlation functions for  $R \gtrsim 0.9 R_{\text{SNR}}$  imply the developed GS95 turbulence that is trans-Alfvénic. If this is the case, the velocity dispersion of the largest eddy,  $u_{\text{inj}}$ , should be close to the Alfvén velocity,  $C_A$ , and it gives the Alfvén Mach number of turbulence,  $M_{A,\text{turb}} \equiv u_{\text{inj}}/C_A \approx 1$ . For comparison, if we consider the SNR shock velocity ( $\approx 5000$  km s $^{-1}$ , e.g. Williams et al. 2016) and the magnetic field strength in the ISM ( $\sim 3$   $\mu\text{G}$ , Myers 1978; Beck 2001), we obtain a high Alfvén Mach number of  $\sim 500$  for the shock. Thus, in comparison with the shock, our results imply smaller gas velocity and/or larger magnetic-field strength at  $R \gtrsim 0.9 R_{\text{SNR}}$ . The non-thermal X-ray filaments with the thickness  $\sim 0.01 R_{\text{SNR}}$  seen in Tycho's SNR imply a significant cooling of high energy CR electrons, suggesting the presence of a strong (likely amplified) magnetic-field (e.g. Bamba et al. 2005).

We discuss how the condition  $M_{A,\text{turb}} \approx 1$  is satisfied at the vicinity of the shock. Multidimensional MHD simulations (e.g. Giacalone & Jokipii 2007; Inoue et al. 2009, 2010, 2012, 2013) showed that the SNR shock is rippled owing to the interaction with density fluctuations pre-existing in the ISM (e.g. Armstrong et al. 1995). Because of the shock rippling, the velocity component tangential to the shock surface is generated downstream, yielding the velocity dispersion just behind the shock (e.g. McKenzie & Westphal 1968; Mahesh et al. 1997; Shimoda et al. 2015). Using three-dimensional MHD simulations, Inoue et al. (2013) showed that the strength of the downstream velocity dispersion  $\Delta u$  can be expressed by using growth velocity of the Richtmyer-Meshkov instability (RMI)  $u_{\text{RMI}}$ :

$$\Delta u \approx u_{\text{RMI}} \approx A \langle u_{\text{sh}} \rangle, \quad (4)$$

where  $A = (\Delta\rho/\langle\rho\rangle)/(1 + \Delta\rho/\langle\rho\rangle)$  is the Atwood number and  $\langle u_{\text{sh}} \rangle$  is the mean shock velocity.  $\Delta\rho$  and  $\langle\rho\rangle$  are the dispersion of upstream density fluctuation and the mean upstream density, respectively. They assumed a weak magnetic field in the upstream region,  $M_A = \langle u_{\text{sh}} \rangle / C_{A,1} \approx 100$ , where  $C_{A,1}$  is the upstream Alfvén speed, and obtained super-Alfvénic turbulence (i.e.  $M_{A,\text{turb}} > 1$ ) behind the shock (though the result depends on  $\Delta\rho$ , see Inoue et al. (2013) for details). The downstream magnetic field is amplified by the turbulent dynamo process induced by the RMI-driven super-Alfvénic turbulence. The amplified field is able to explain the orientations of observed magnetic fields in young SNRs (e.g. Dickel & Milne 1976; Dickel et al. 1991; Reynolds & Gilmore 1993; DeLaney et al. 2002; Reynoso et al. 2013).

The field amplification becomes significant at a distance

$$d_{\text{RMI}} \approx l_{\Delta\rho} / (r_c A), \quad (5)$$

from the shock front (e.g. Richtmyer 1960; Sano et al. 2012; Inoue et al. 2013), where  $l_{\Delta\rho}$  is the scale length of upstream density fluctuations and  $r_c$  is the shock compression ratio. Williams et al. (2013) examined the ambient density of Tycho's SNR from infrared dust emissions and found order-of-magnitude variations in density at the scale length of  $l_{\Delta\rho} \sim R_{\text{SNR}}$ . Such density variations are also inferred by observations of the expansion rate of Tycho's SNR (Williams et al. 2016). Their results imply  $A \approx 1$  on the scale  $l_{\Delta\rho} \sim R_{\text{SNR}}$ , giving  $d_{\text{RMI}} \sim 0.2 R_{\text{SNR}}(l_{\Delta\rho}/R_{\text{SNR}})(r_c/4)^{-1}$ . Thus, the magnetic field amplification through the turbulent dynamo induced by the RMI-driven turbulence may explain the condition  $M_{\text{A,turb}} \approx 1$  at  $R \sim 0.9 R_{\text{SNR}}$  from the shock front by this orders-of-magnitude estimation, which is consistent with our results for Tycho's SNR.

Our results for the inner circles ( $R \lesssim 0.9 R_{\text{SNR}}$ ), which show somewhat flatter spectra than the outer ( $R \gtrsim 0.9 R_{\text{SNR}}$ ) ones at relatively large scales  $\lambda/R \gtrsim 0.2$ , may be ascribed to the interaction between the well-developed GS95 turbulence and the RTI driven turbulence. To examine this interpretation, MHD simulations solving the interaction between the well-developed GS95 turbulence and the RTI driven turbulence are required. We will study this in forthcoming paper.

There are other possibilities to amplify the magnetic field at the vicinity of the shock such as the Bell instability (Bell 2004), which is usually expected as the mechanism responsible for the magnetic field amplification at the *upstream* region leading to the acceleration of knee-energy CR protons. This instability occurs resulting from the interaction between leaking CRs from the shock and the background plasma. If the upstream field has been already amplified, the trans-Alfvénic condition can be satisfied in the region just behind the shock. This situation may be consistent with our results for Tycho's SNR. Moreover, the leaking CRs excite an acoustic instability (enhance a compressible perturbation, e.g. Drury & Falle 1986). The upstream plasma affected by the leaking CRs, i.e. shock precursor, interacts with the density fluctuations pre-existing in the ISM. This interaction also leads to the field amplification by a turbulent dynamo process in the upstream region (Beresnyak et al. 2009; del Valle et al. 2016). Indeed, Xu & Lazarian (2017) pointed out that the shock crossing time of the precursor length is large enough to lead to full development of the precursor dynamo in partially ionized ISM. Note that the Balmer line emissions from Tycho's SNR indicate the interaction between the shock and the partially ionized ISM (e.g. Chevalier et al. 1980; Lee et al. 2007).

The above possible amplification mechanisms predict different evolution tracks of the magnetic energy spectrum. For the RMI inducing amplification on the down-side (i.e. turbulent dynamo in super-Alfvénic turbulence), magnetic field disturbances on the scales larger than  $l_A$ , at which the turbulent velocity is equal to the Alfvén velocity, grow with time (e.g. Cho & Vishniac 2000a; Brandenburg & Subramanian 2005; Xu & Lazarian 2016). It indicates that the  $l_A$  evolves toward a larger scale with increasing a distance from the shock front. On the other hand, if the field has significantly been amplified upstream, such evolution would not be seen. Moreover, Pohl et al. (2005) pointed out that the field amplified by the Bell instability damps downstream. Therefore, we can assess the real amplification mechanism from the spatial variation of the mag-

netic energy spectrum. The correlation for the most outer circle with the radius  $R = 1.00R_{\text{SNR}}$  roughly shows the single power-law with the Kolmogorov-like scaling, which favors an well-amplified field just behind the shock, i.e. the upstream field amplification. It would be confirmed once the evolution track of spectrum within the most outer circle is resolved.

Supposing that the strength of amplified magnetic field is  $\sim 100 \mu\text{G}$  (e.g. Parizot et al. 2006), the scale length of the gyroradius of the knee-energy CRs,  $r_{g,\text{knee}} \sim 0.01 \text{ pc} \left(\frac{E}{10^{15.5} \text{ eV}}\right) \left(\frac{B}{100 \mu\text{G}}\right)^{-1}$ , is shorter than the spatial resolution of the present data. The scale length of  $r_{g,\text{knee}}$  will be resolved and the mechanism of field amplification may be distinguished, if we have data of higher spatial resolution (say,  $\lesssim 0.001R_{\text{SNR}}$ ). Once we obtain the magnetic energy spectrum at the length scale less than  $r_{g,\text{knee}}$ , we can estimate the diffusion coefficient of the knee-energy CRs and the possibilities of their acceleration in SNR. We thus need a higher sensitivity with sub arcsecond resolution at GHz band; this would be a science case of the Square Kilometre Array (SKA).

Finally, our method would be available not only for SNRs but also other astrophysical objects with a spherical-shell structure, such as radio relics in galaxy clusters.

## ACKNOWLEDGEMENTS

We are grateful Dr. Brian J. Williams who kindly provided us with the VLA image used in this paper. We thank Prof. Jungyeon Cho for valuable comments to complete this work. We also thank the anonymous referee for his/her comments to further improve the paper. This work is supported by Grant-in-aids for JSPS Fellows (15J08894, JS) and JSPS KAKENHI Grants: 15H03639, 15K17614, 17H0110 (TA), 15K05039 (TI), and 15K05080 (YF).

## REFERENCES

- Akahori T., et al., 2018, *PASJ*, **70**, R2  
 Archambault S., et al., 2017, *ApJ*, **836**, 23  
 Armstrong J. W., Rickett B. J., Spangler S. R., 1995, *ApJ*, **443**, 209  
 Bamba A., Yamazaki R., Yoshida T., Terasawa T., Koyama K., 2005, *ApJ*, **621**, 793  
 Beck R., 2001, *Space Sci. Rev.*, **99**, 243  
 Bell A. R., 1978, *MNRAS*, **182**, 147  
 Bell A. R., 2004, *MNRAS*, **353**, 550  
 Beresnyak A., Jones T. W., Lazarian A., 2009, *ApJ*, **707**, 1541  
 Blandford R., Eichler D., 1987, *Phys. Rep.*, **154**, 1  
 Blandford R. D., Ostriker J. P., 1978, *ApJ*, **221**, L29  
 Brandenburg A., Subramanian K., 2005, *Phys. Rep.*, **417**, 1  
 Chepurinov A. V., 1998, *Astronomical and Astrophysical Transactions*, **17**, 281  
 Chevalier R. A., Kirshner R. P., Raymond J. C., 1980, *ApJ*, **235**, 186  
 Cho J., Lazarian A., 2003, *MNRAS*, **345**, 325  
 Cho J., Lazarian A., 2010, *ApJ*, **720**, 1181  
 Cho J., Vishniac E. T., 2000a, *ApJ*, **538**, 217  
 Cho J., Vishniac E. T., 2000b, *ApJ*, **539**, 273  
 DeLaney T., Koralesky B., Rudnick L., Dickel J. R., 2002, *ApJ*, **580**, 914  
 Dickel J. R., Milne D. K., 1976, *Australian Journal of Physics*, **29**, 435

Dickel J. R., van Breugel W. J. M., Strom R. G., 1991, *AJ*, **101**, 2151

Drury L. O., Falle S. A. E. G., 1986, *MNRAS*, **223**, 353

Getmantsev G. G., 1959, *Soviet Ast.*, **3**, 415

Giacalone J., Jokipii J. R., 2007, *ApJ*, **663**, L41

Goldreich P., Sridhar S., 1995, *ApJ*, **438**, 763

Green D. A., 2009, *Bulletin of the Astronomical Society of India*, **37**, 45

Hayato A., et al., 2010, *ApJ*, **725**, 894

Inoue T., Yamazaki R., Inutsuka S.-i., 2009, *ApJ*, **695**, 825

Inoue T., Yamazaki R., Inutsuka S.-i., 2010, *ApJ*, **723**, L108

Inoue T., Yamazaki R., Inutsuka S.-i., Fukui Y., 2012, *ApJ*, **744**, 71

Inoue T., Shimoda J., Ohira Y., Yamazaki R., 2013, *ApJ*, **772**, L20

Jokipii J. R., 1966, *ApJ*, **146**, 480

Katsuda S., Petre R., Hughes J. P., Hwang U., Yamaguchi H., Hayato A., Mori K., Tsunemi H., 2010, *ApJ*, **709**, 1387

Kolmogorov A., 1941, *Akademiia Nauk SSSR Doklady*, **30**, 301

Lazarian A., 2006, *ApJ*, **645**, L25

Lazarian A., Pogosyan D., 2012, *ApJ*, **747**, 5

Lazarian A., Pogosyan D., 2016, *ApJ*, **818**, 178

Lazarian A., Vishniac E. T., 1999, *ApJ*, **517**, 700

Lee J.-J., Koo B.-C., Raymond J., Ghavamian P., Pyo T.-S., Tajitsu A., Hayashi M., 2007, *ApJ*, **659**, L133

Lee H., Lazarian A., Cho J., 2016, *ApJ*, **831**, 77

Mahesh K., Lele S. K., Moin P., 1997, *Journal of Fluid Mechanics*, **334**, 353

McKenzie J. F., Westphal K. O., 1968, *Physics of Fluids*, **11**, 2350

Myers P. C., 1978, *ApJ*, **225**, 380

Parizat E., Marcowith A., Ballet J., Gallant Y. A., 2006, *A&A*, **453**, 387

Pohl M., Yan H., Lazarian A., 2005, *ApJ*, **626**, L101

Reynolds S. P., Gilmore D. M., 1993, *AJ*, **106**, 272

Reynoso E. M., Hughes J. P., Moffett D. A., 2013, *AJ*, **145**, 104

Richtmyer R. D., 1960, *CPA*, **13**, 297

Ruiz-Lapuente P., et al., 2004, *Nature*, **431**, 1069

Sano T., Nishihara K., Matsuoka C., Inoue T., 2012, *ApJ*, **758**, 126

Shimoda J., Inoue T., Ohira Y., Yamazaki R., Bamba A., Vink J., 2015, *ApJ*, **803**, 98

Vladimirov A. E., Bykov A. M., Ellison D. C., 2009, *ApJ*, **703**, L29

Warren J. S., et al., 2005, *ApJ*, **634**, 376

Williams B. J., Borkowski K. J., Ghavamian P., Hewitt J. W., Mao S. A., Petre R., Reynolds S. P., Blondin J. M., 2013, *ApJ*, **770**, 129

Williams B. J., Chomiuk L., Hewitt J. W., Blondin J. M., Borkowski K. J., Ghavamian P., Petre R., Reynolds S. P., 2016, *ApJ*, **823**, L32

Xu S., Lazarian A., 2016, *ApJ*, **833**, 215

Xu S., Lazarian A., 2017, *ApJ*, **850**, 126

del Valle M. V., Lazarian A., Santos-Lima R., 2016, *MNRAS*, **458**, 1645

## APPENDIX A: MEASURING METHOD OF MAGNETIC FIELD CORRELATION

Here we provide the measuring method of magnetic energy spectrum in SNRs by applying the method developed for the ISM.

Lazarian & Pogosyan (2012, 2016) provided a mathematical formalism describing how second order correlation functions of synchrotron intensities are related with magnetic field disturbances. An emissivity of a synchrotron emission per frequency  $\nu$  depends on the strength of magnetic field component perpendicular to the line of sight,  $|\mathbf{B}_n| = B_n$ ,

as

$$\begin{aligned} i_\nu(\mathbf{r}) &= K\nu^{-\alpha} B_n(\mathbf{r})^{1+\alpha}, \\ &= K\nu^{1-\gamma} B_n(\mathbf{r})^\gamma, \end{aligned} \quad (\text{A1})$$

where  $K$  is a function depending on the density of relativistic electrons,  $\alpha = (s - 1)/2$ ,  $s$  is the power-law index of the CR electron energy spectrum and we have defined  $\gamma \equiv 1 + \alpha$  for simplicity. Thus, the second-order correlation function of the synchrotron emissivity,

$$C_{i_\nu, \gamma}^{(2)}(\mathbf{l}) = \langle i_\nu(\mathbf{r}) i_\nu(\mathbf{r} + \mathbf{l}) \rangle_{\mathbf{r}}, \quad (\text{A2})$$

is related with the magnetic field correlation as

$$C_{i_\nu, \gamma}^{(2)}(\mathbf{l}) \propto \langle B_n(\mathbf{r})^\gamma B_n(\mathbf{r} + \mathbf{l})^\gamma \rangle_{\mathbf{r}}. \quad (\text{A3})$$

When  $\gamma = 1$ , which is equivalent to  $\alpha = 0$  and  $s = 1$ , and spatial distribution of CR electrons is uniform (i.e.  $K$  is constant),  $C_{i_\nu, \gamma}^{(2)}$  becomes identical to the magnetic field correlation function. The case of  $\gamma = 2$  ( $\alpha = 1$  and  $s = 3$ ) is also simple and can be representative for the case of arbitrary  $\gamma$ . Omitting the notations as  $B_n(\mathbf{r}) \rightarrow B_n$  and  $B_n(\mathbf{r} + \mathbf{l}) \rightarrow B'_n$ , we obtain

$$\langle B_n^2 B_n'^2 \rangle_{\mathbf{r}} = \frac{\langle B_n^4 + B_n'^4 \rangle_{\mathbf{r}}}{2} - \frac{1}{2} \langle (B_n + B'_n)^2 (B_n - B'_n)^2 \rangle_{\mathbf{r}}. \quad (\text{A4})$$

If we decompose the magnetic field into the mean component  $\bar{B}_n = \langle B_n \rangle_{\mathbf{r}}$  and the fluctuating component  $\Delta B_n = B_n - \bar{B}_n$ , the above equation can be written as

$$\begin{aligned} \langle B_n^2 B_n'^2 \rangle_{\mathbf{r}} &= \frac{\langle B_n^4 + B_n'^4 \rangle_{\mathbf{r}}}{2} \\ &- 2\bar{B}_n^4 \left\langle \left( 1 + \frac{\Delta B_n + \Delta B'_n}{\bar{B}_n} \right)^2 \left( \frac{\Delta B_n - \Delta B'_n}{\bar{B}_n} \right)^2 \right\rangle_{\mathbf{r}}. \end{aligned} \quad (\text{A5})$$

For small standard deviation of the field  $\sqrt{\langle (B_n - \bar{B}_n)^2 \rangle_{\mathbf{r}}} / \bar{B}_n \sim |(\Delta B_n + \Delta B'_n) / \bar{B}_n| < 1$ , the correlation function of  $B_n^2$  becomes

$$\begin{aligned} \langle B_n^2 B_n'^2 \rangle_{\mathbf{r}} &\approx \frac{\langle B_n^4 + B_n'^4 \rangle_{\mathbf{r}}}{2} - 2\bar{B}_n^4 \left\langle \left( \frac{\Delta B_n - \Delta B'_n}{\bar{B}_n} \right)^2 \right\rangle_{\mathbf{r}} \\ &= 4\bar{B}_n^2 \langle \Delta B_n \Delta B'_n \rangle_{\mathbf{r}} + \text{const.}, \end{aligned} \quad (\text{A6})$$

where we have assumed the isotropic turbulent field as  $\langle B_n^4 \rangle_{\mathbf{r}} = \langle B_n'^4 \rangle_{\mathbf{r}}$  and  $\langle \Delta B_n^2 \rangle_{\mathbf{r}} = \langle \Delta B_n'^2 \rangle_{\mathbf{r}}$ . Thus,  $\langle B_n^2 B_n'^2 \rangle_{\mathbf{r}}$  reproduces the second-order correlation function of the magnetic field disturbances. Note that even if we consider a completely random field, this approximation would be applicable for small scales. This is because the field disturbances on the larger scales act as a guide field for the field disturbances on the smaller scales (see, e.g. Cho & Vishniac 2000b). Lazarian & Pogosyan (2012) showed that

$$\frac{\langle B_n^2 B_n'^2 \rangle_{\mathbf{r}}}{\langle B_n^4 \rangle_{\mathbf{r}} - \langle B_n^2 \rangle_{\mathbf{r}}^2} \approx \frac{\langle B_n^\gamma B_n'^\gamma \rangle_{\mathbf{r}}}{\langle B_n^{2\gamma} \rangle_{\mathbf{r}} - \langle B_n^\gamma \rangle_{\mathbf{r}}^2}, \quad (\text{A7})$$

for several  $\gamma$  for a power-law correlation function of  $B_n$ . In the range of  $1.2 \leq \gamma \leq 3$ , they reported that the maximum difference of  $\langle B_n^\gamma B_n'^\gamma \rangle_{\mathbf{r}}$  from  $\langle B_n^2 B_n'^2 \rangle_{\mathbf{r}}$  is only 3%. This suggests that the correlation functions can be written as

$$\langle B_n(\mathbf{r})^\gamma B_n(\mathbf{r} + \mathbf{l})^\gamma \rangle_{\mathbf{r}} \approx \mathcal{P}(\gamma) \langle B_n(\mathbf{r})^2 B_n(\mathbf{r} + \mathbf{l})^2 \rangle_{\mathbf{r}}, \quad (\text{A8})$$

where  $\mathcal{P}$  is a function of  $\gamma$ . This argument is numerically confirmed by Lee et al. (2016). They performed synthetic

observations of synchrotron emissions from simulated magnetic field and derived the Fourier power spectrum from the correlation of the observed synchrotron polarization intensity for the parameter range  $1.5 \leq \gamma \leq 4$ . They found that the power spectrum reproduced the spectral index of the given magnetic field. For SNRs, observations of the radio synchrotron intensity per frequency show the power-law spectrum with the index  $\alpha \approx 0.6$  that indicates  $\gamma \approx 1.6$  and  $s \approx 2.2$  (e.g. Green 2009). Hence,  $C_{i,\gamma}^{(2)}$  can reproduce the second-order correlation function of magnetic field disturbance in the SNRs.

In order to measure the second-order correlation function of magnetic field disturbance from the synchrotron emissions, we must consider the projection effect. We define the observed intensity of synchrotron emission per frequency at the two-dimensional sky position  $\mathbf{X} = (x, y)$  as

$$I_\nu(\mathbf{X}) = \int_0^{L(\mathbf{X})} K \nu^{1-\gamma} B_n(\mathbf{X}, z)^\gamma dz, \quad (\text{A9})$$

where  $z$  represents the coordinate along the line of sight and  $L(\mathbf{X})$  is the extent of the emission region. Note that  $L$  is a function of  $\mathbf{X}$  in general. The second-order correlation function for  $I_\nu$  is written as

$$\begin{aligned} C_{I_\nu}^{(2)}(\boldsymbol{\lambda}) &= \frac{\int I_\nu(\mathbf{X}) I_\nu(\mathbf{X}') d^2\mathbf{X}}{\int d^2\mathbf{X}} \\ &\equiv \langle I_\nu(\mathbf{X}) I_\nu(\mathbf{X} + \boldsymbol{\lambda}) \rangle_{\mathbf{X}}, \end{aligned} \quad (\text{A10})$$

where  $\boldsymbol{\lambda} \equiv \mathbf{X}' - \mathbf{X}$  is the position vector of two separated positions in the sky  $\mathbf{X}$  and  $\mathbf{X}'$  (see also Eq. (2) of the main text). The correlation function can be represented as

$$\begin{aligned} C_{I_\nu}^{(2)}(\boldsymbol{\lambda}) &= K \nu^{1-\gamma} \int_0^{L(\mathbf{X})} dz \int_0^{L'(\mathbf{X}')} dz' \\ &\quad \times \langle B_n(\mathbf{X}, z)^\gamma B_n(\mathbf{X} + \boldsymbol{\lambda}, z')^\gamma \rangle_{\mathbf{X}}. \end{aligned} \quad (\text{A11})$$

For the constant  $L(\mathbf{X}) = L_0$ , Lazarian & Pogosyan (2016) and Lee et al. (2016) demonstrated that  $C_{I_\nu}^{(2)}$  reproduces the scaling relation of a given magnetic field correlation. However, if  $L$  varies spatially,  $C_{I_\nu}^{(2)}$  is affected by the geometrical structure of the emission region, which is usually unknown. However, fortunately, the emission regions of some young SNRs are known to be a spherical shell (e.g. Dickel et al. 1991; Reynoso et al. 2013). Therefore, if we select the points  $\mathbf{X}$  and  $\mathbf{X}'$  on the concentric circle of SNR image, the condition of  $L(\mathbf{X}) = \text{constant}$  is satisfied. In Figure A1, we show a schematic of the SNR shell and projected image.

This paper has been typeset from a  $\text{\TeX}/\text{\LaTeX}$  file prepared by the author.

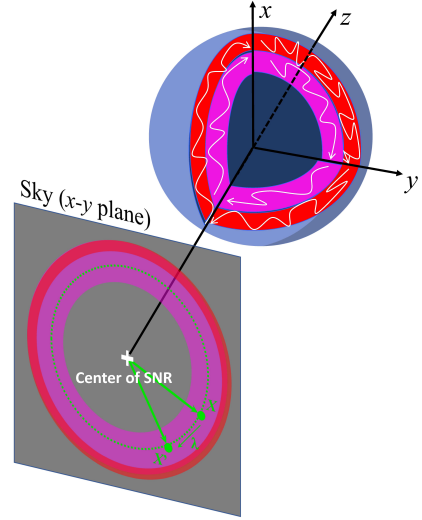


**Figure A1.** Schematic of SNR shell and projected image. The blue spherical shell with partial cross sections shows the SNR shell. The line of sight is along the  $z$ -axis, and the  $x$ - $y$  plane corresponds to the projected sky. The white lines schematically represent turbulent magnetic field lines. The synchrotron emissions from turbulent media are projected onto the sky (the red and magenta toruses). The white cross indicates the center of the SNR. If we analyse the intensity correlation between positions  $\mathbf{X}$  and  $\mathbf{X}' = \mathbf{X} + \boldsymbol{\lambda}$  on the concentric circle (the green dots), the line of sight extent  $L(\mathbf{X})$  becomes constant and the correlation function is not affected by the structure of SNR shell.